frontiers in Earth Science

ORIGINAL RESEARCH
published: 29 January 2021
doi: 10.3389/feart.2020.586279

Short-Term Seismic Precursor Anomalies of Hydrogen Concentration in Luojishan Hot Spring Bubbling Gas, Eastern Tibetan Plateau

Xiaocheng Zhou, Yucong Yan, Wenya Fang, Wanli Wang, Hongyu Shi and Pengfei Li*

Institute of Earthquake Forecasting, China Earthquake Administration, Beijing, China

The gas compositions (He, H_2, CO_2, CH_4, Ar and N_2) and isotope ratios ($^3He/^4He$ and $\delta^{13}C$) were yearly investigated from April 2010 to April 2019 at the Luojishan spring located in the proximity of the Zemuhe Fault, eastern Tibetan Plateau. The continuous automatic monitoring of hydrogen concentrations in Luojishan hot spring bubbling gas for the purpose of earthquake prediction requires the discrimination of seismic precursor anomalies. Helium isotope ratios ($^3He/^4He$) in the bubbling gas of hot springs varied from 0.05 to 0.18 Ra (Ra = $^3He/^4He = 1.39 \times 10^{-6}$ in the air), with a maximum mantle-derived He up to 2.2% of the total He measured in the Luojishan hot spring (assuming R/Ra = 8.0 for mantle). This suggests that Zemuhe Fault might act as a conduit for crustal-derived fluid. N_2 concentrations in the majority of the hot spring was ≥80 vol%, and $\delta^{13}C_{CO2}$ values varied from −13.2 to −9.3‰ (vs.PDB). Hydrogen concentration time series display a complex temporal pattern reflecting a wide range of different physical processes. There were short-term (5–60 h) seismic precursor anomalies of hydrogen concentration before natural earthquake. The anthropogenically-induced earthquakes provoke only post-earthquake responses. The concentration of hydrogen in bubbling gas of the Luojishan hot spring is sensitive to increase of stress in the Xianshuihe-Xiaojiang fault system. Monitoring the hydrogen concentrations with automatic gas stations may be promising tool for unraveling earthquake mechanisms and for predicting earthquakes.

Keywords: hydrogen, hot spring, zemuhe fault, earthquake forecasting, seismic precursor

OPEN ACCESS

Edited by:
Giovanni Martinelli,
National Institute of Geophysics and Volcanology, Italy

Reviewed by:
Zheming Shi,
China University of Geosciences, China
Selin Süer,
Middle East Technical University, Turkey

****Correspondence:***
Xiaocheng Zhou
zhouxiaocheng188@163.com

Specialty section:
This article was submitted to Geochemistry, a section of the journal Frontiers in Earth Science

Received: *22 July 2020*
Accepted: *23 December 2020*
Published: *29 January 2021*

Citation:
Zhou X, Yan Y, Fang W, Wang W, Shi H and Li P (2021) Short-Term Seismic Precursor Anomalies of Hydrogen Concentration in Luojishan Hot Spring Bubbling Gas, Eastern Tibetan Plateau. Front. Earth Sci. 8:586279. doi: 10.3389/feart.2020.586279

INTRODUCTION

Earthquake precursors are elusive, and this elusiveness has hampered earthquake prediction (Donald, 1988; Cicerone et al., 2009; Gherardi et al., 2017). The high uncertainty and low predictability of earthquakes during forecasting make earthquakes one of the worst natural disasters, which may lead to the instant loss of lives and properties (Gupta, 2001; Wen et al., 2008). The anomalously high concentration of helium, hydrogen, carbon dioxide and radon in hot spring bubbling gas have been widely studied in seismically active faults in recent years, especially in Japan, China, Italy and United States, in hunt of changes that might be premonitory of for earthquake prediction (King, 1986; Sugisaki and Sugiura, 1986; Nagamine, 1994; Cicerone et al., 2009; Babuška et al., 2016; Weinlich et al., 2016; Fischer et al., 2017; Huang et al., 2017). Temporal abnormal variations of gas (He, H_2, CO_2, Rn, CH_4) concentration have been observed with durations of a few hours to several days before and after a lot of large earthquakes at some gas monitoring stations at the

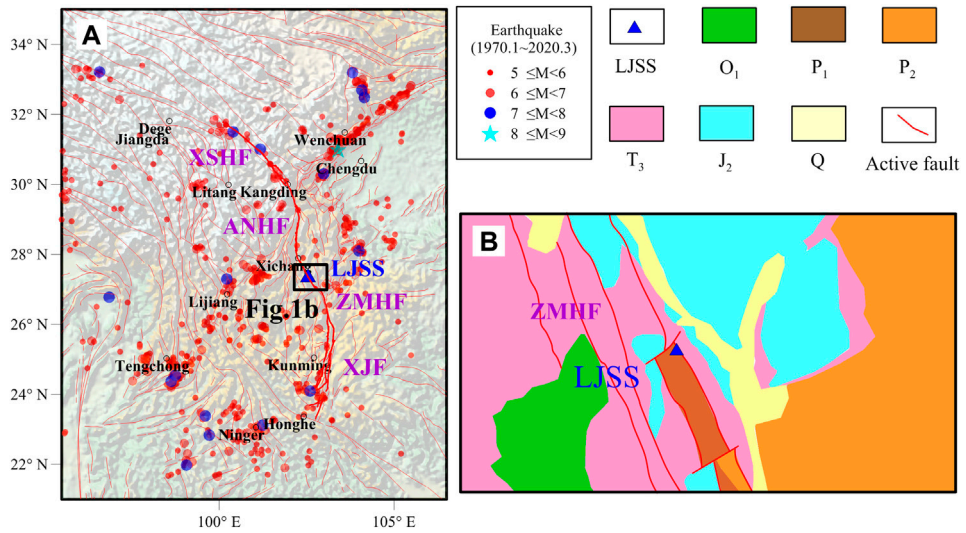

FIGURE 1 | Location of the Luojishan station (LJSS) **(A)** Topographic map of the east Tibetan Plateau. **(B)** Geological map of the Luojishan station and around are shown in **(A)**. Abbreviations: LMSF, Longmenshan Fault; ANHF, Anninghe Fault; XSHF, Xianshuihe Fault; ZMHF, Zemuhe Fault; XJF, Xiaojiang Fault.

epicentral distances of up to several hundreds of kilometers, which are usually related to the chemical and physical changes occurring in the active faults as enhanced/reduced water–rock interaction, crustal stress/strain, permeability structure, etc. before and after earthquakes (Sugisaki et al., 1983, 1996; Cicerone et al., 2009; Umeda et al., 2013; Weinlich et al., 2016). The large change of gas geochemical anomalies as regards shape, duration, delay/anticipation time and parameters-association with respect to foreshocks, main-shock and aftershocks are considered to be highly site specific (King, 1986; Sugisaki et al., 1996).

Noble gas and their isotopes are very good natural tracers for exploring crust-mantle interaction in different geologic background because they are chemically inert and thus their isotopic signature is conservative with respect to the source of gas/fluid in crustal water-rock interactions (Sano and Wakita., 1985; Hilton, 1996). The helium isotopes can provide clear evidence for the existence of mantle-derived fluids in the crust, ^{3}He is retained in the Earth's interior and essentially primordial, whereas ^{4}He is mainly produced in the crust by the decay of U and Th (Hilton, 1996; Hilton, 2007). The isotopic signatures of He showed some correlations with seismic activities (Sano and Marty, 1995; Kissin, 2007).

Hydrogen could play a very important role in mechanisms of process taking place in both the shallow and deep reservoirs (Zgonnik, 2020). Hydrogen in hot spring bubbling gas in active faults may be used in monitoring of earthquakes (Wakita et al., 1980; Sato et al., 1986). The increase of H_2 concentration may be correlated with 11 $M \geq 5$ earthquakes at some sites in the San Andreas Fault between July 1982 and November 1983 (Sato et al., 1986). The premonitory increases of the H_2 concentration in the bubbling gas of hot spring are geochemical signals of the earthquake nucleation process of stress-corrosion mechanism. In other words, aseismic slips before earthquakes might have enhanced H_2 production in pre-existing active fault planes by mechanochemical reaction of newly formed surface from fractured rock surface with water (Ito et al., 1999).

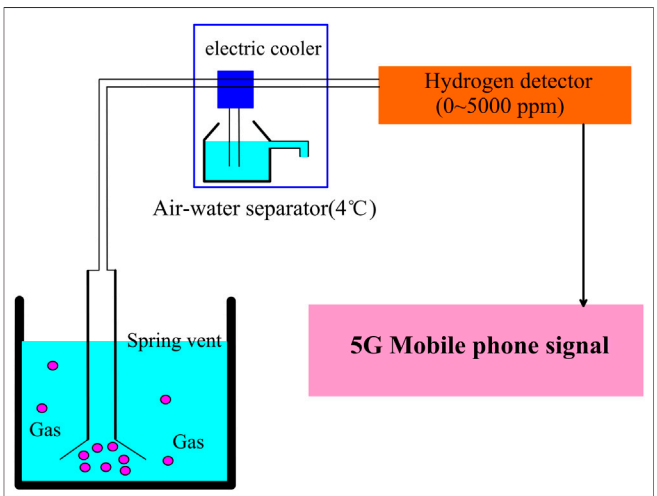

FIGURE 2 | Schematic diagram of H_2 concentration monitoring station.

The aim of this research was to 1) monitor the variations of gas and isotope composition at the Luojishan hot spring before, during and after seismic events, and 2) characterize the short-term seismic precursor anomalies of hydrogen concentration, 3) distinguish between the anomalies of hydrogen concentration induced by natural earthquake from the anomalies induced by anthropogenically-induced earthquakes.

Geological Setting

A huge left-lateral strike-slip active fault system in the eastern boundary of the Sichuan-Yunnan rhombus block in southwestern China contains four major faults named Anninghe Fault (ANHF), Zemuhe Fault (ZMHF), Xianshuihe Fault (XSHF), and Xiaojiang Fault (XJF), where the strongest seismicity in continental China occurs (Wen et al., 2008; Zhang, 2013). The ZMHF strikes

TABLE 1 | Gas and isotopic compositions of the Luojishan hot spring.

NO	Date		He	H_2	CO_2	CH_4	N_2	O_2	Ar	$^3He/^4He$	$^3He/^4He$		$\delta^{13}C_{CO2}$	$He_{mantle\text{-}derived}$
	(yyyy/mm/dd)		(ppm)	(ppm)	(%)	(%)	(%)	(%)	(%)	(R/Ra)	(Rc/Ra)	$^4He/^{20}Ne$	(‰)	(%)
1[a]	2008/6/20	T	1810.0		11.32		83.50	4.09	0.99	0.22			−11.2	
2[a]	2008/10/29	(℃)	1650.0		11.28		85.25	2.47	1.00	0.04	0.04	102.6	−12.2	0.47
3[a]	2009/6/22	43.8	1720.0		10.14	0.28	84.56	3.93	0.98	0.07	0.06	117.4	−10.8	0.80
4	2010/4/25	43.6	1540.0		10.44	0.00	86.15	2.30	0.99	0.05	0.05	99.1	−10.8	0.63
5	2010/6/16	44.0	1371.0		12.58	0.00	82.53	3.80	0.94	0.18	0.17	74.9	−10.8	2.16
6	2013/5/11	43.0	632.6	1.00	13.28		81.42	1.97	1.13	0.08	0.07	112.2	−9.3	0.91
7	2014/9/2	44.8	1800.0	0.00	7.42	0.04	90.69	0.37	1.23	0.05	0.05	83.6	−9.5	0.58
8	2015/7/18	44.5	1124.6	1.30	11.47	0.00	87.47	1.10	0.22	0.07	0.07	111.6	−10.6	0.85
9	2016/1/17	44.5	1279.5	1.00	12.66		83.51	1.35	1.26	0.06	0.05	37.3	−9.3	0.67
10	2017/1/8	44.5	1305.9	2.00	9.26	0.01	87.81	0.22	0.24	0.06	0.06	60.4	−11.8	0.69
11	2018/3/7	44.8	1483.0	1.00	13.06		83.45	0.16	0.93	0.06	0.06	96.7	−9.7	0.71
12	2019/4/19	43.3	1532.0	1.00	10.84	0.02	85.16	0.49	0.93	0.07	0.07	104.0	−13.2	0.84

[a]*Data come from Zhou et al. (2015).*

NNW–SSE and extends for about 120 km, which intersects the N–S-trending ANHF and XJF at an acute angle (**Figure 1**). The strain energy were released by the form of repeated large earthquakes in the ZMHF, which are caused by the southeastwards motion of the Tibetan Plateau (Ren et al., 2010).

Quaternary alluvial deposits are composed mainly of fine sand, sandy gravel, silt, and clay, and are widely distributed in the Luojishan hot spring. Cenozoic strata (Late Tertiary to Early Quaternary) consist mainly of interbedded sandstones and mudstones with thin layers of coal. The basement rock along the ZMHF consists mainly of metamorphic rocks including Pre-Cambrian rhyolite and granite, and Permian basalt and Triassic granite (He and Oguchi, 2008; Ren et al., 2010).

Historical earthquake records show there are three strong earthquakes over the last millennium in the ZMHF: the 814AD *M* 7.0 earthquake, and the 1536 *M* 7.5 earthquakes, and 1850 *M*7.5 Xichang earthquake (Wen et al., 2008). The historical seismicity indicates that the ZMHF is still active and the probability of a strong earthquake in the future is high (Wen et al., 2008; Ren et al., 2010).

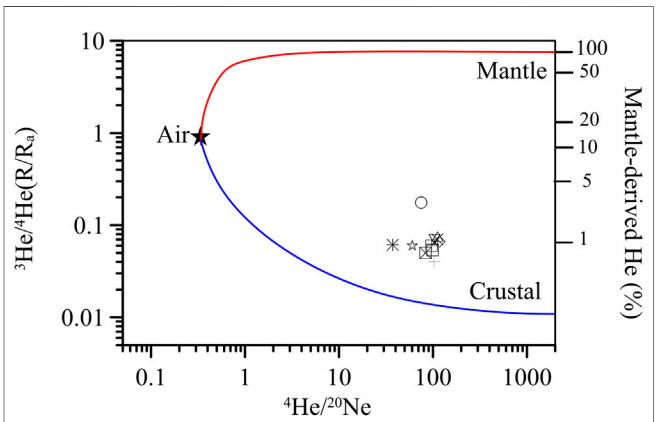

FIGURE 3 | Diagram of $^4He/^{20}Ne$ vs. $^3He/^4He$ (R/Ra) ratios. Mixing lines between the upper mantle and atmosphere , and the crust and atmosphere were calculated using the end members:upper mantle ($^4He/^{20}Ne$ = 100,000, $^3He/^4He = 12 \times 10^{-6}$) (Graham 2002), air ($^4He/^{20}Ne$ = 0.318, $^3He/^4He = 1.4 \times 10^{-6}$) (Ozima and Podosek, 1983), continental crust ($^4He/^{20}Ne$ = 100,000, $^3He/^4He = 0.02 \times 10^{-6}$) (Ballentine et al., 2005).

METHOD

Hot Spring Gas Sampling

Gas samples were nine times collected in Luojishan hot spring, using cylindroid bottles (500 ml) made of soda-lime glass from April 25, 2010 to April 19, 2019 (Zhou et al., 2017). The bubbling gas samples were immediately sent to the Key Laboratory of Petroleum Resources Research, Northwest Institute of Eco-Environment and Resources. The measurement of all samples was finished in 30 days.

The temperatures of Luojishan hot spring water were measured with a thermometer having an accuracy of 0.1°C. The composition of gas samples from Luojishan hot spring were analyzed with a Agilent Macro 3000 gas chromatography (Zhou et al., 2015; Zhou et al., 2020). Helium and Neon isotopes in the gas samples were measured using the Noblesse noble gas mass spectrometer. $^3He/^4He$ (R) > 1×10^{-7}, with a precision of ±10%, $1 \times 10^{-8} < {}^3He/^4He$ (R) < 1×10^{-7}, with a precision of ±15% (Cao et al., 2018). The measurements were normalized to standard atmospheric value. Carbon dioxide isotopic compositions in the bubbling gas samples were analyzed by the stable isotope ratio mass spectrometer (Thermo-Fisher Scientific Delta Plus XP) and the GC-IRMS analytical system gas chromatography (Agilent 6890) (Li et al., 2014). The values of $\delta^{13}C$ had a precision of ±0.5‰, and are reported relative to PDB in per mill (Li et al., 2014) .

Hydrogen Concentration of Hot Spring Gas

The continuous hydrogen monitoring was conducted in the Luojishan station at the middle of the XSHF-XJF system (**Figure 2**), which could monitor more earthquakes. The monitor environment is very stable. There is no industrial activity and mining around the monitor station. The depth of the hot spring pool is 1 m. The bubbling gas was collected by a

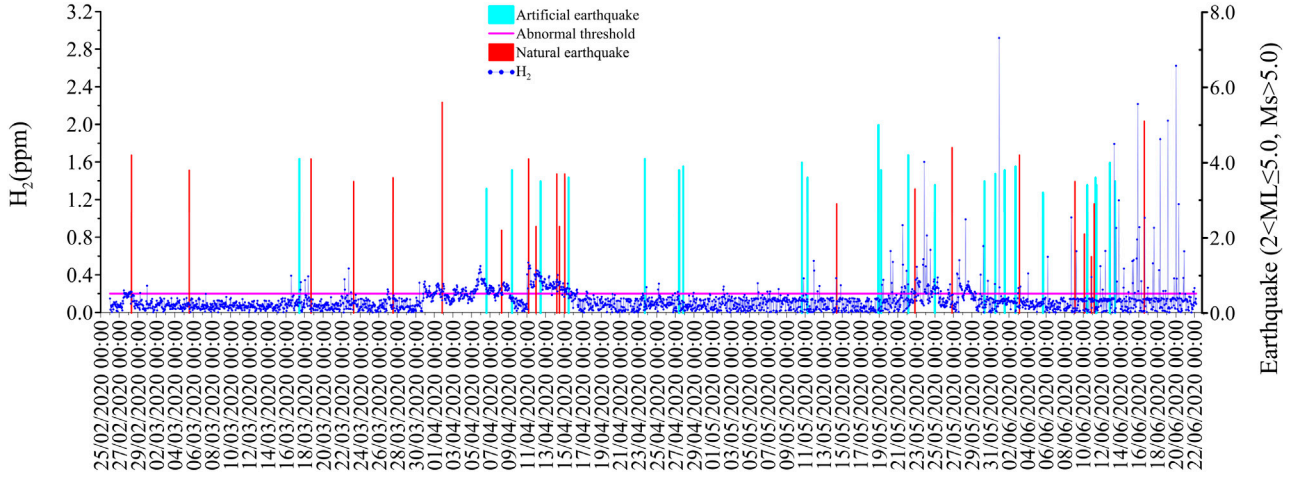

FIGURE 4 | Temporal variations of H_2 concentration in bubbling gas.

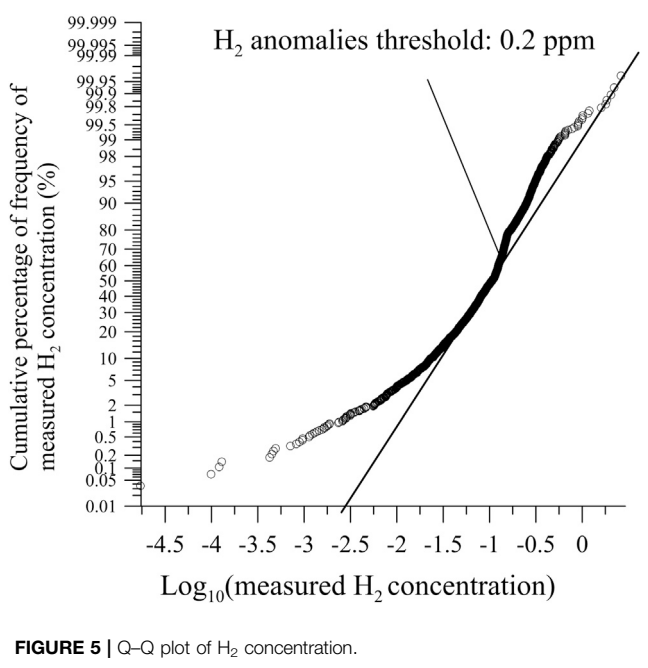

FIGURE 5 | Q–Q plot of H_2 concentration.

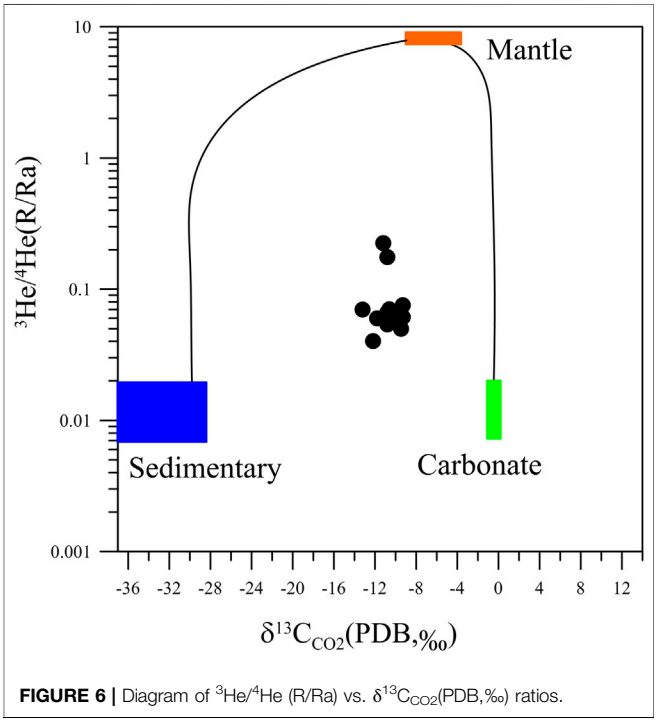

FIGURE 6 | Diagram of $^3He/^4He$ (R/Ra) vs. $\delta^{13}C_{CO2}$(PDB,‰) ratios.

funnel submerged at a depth of 1 m underwater (**Figure 2**). The bubbling gas was accumulated by a polytetrafluoroethylene (PTFE) pipe (length, $2m\times Ø_{outer\ diameter}$,$8cm\times Ø_{inner\ diameter}$, 6 cm). The humidity in the collected gas was reduced by an electric cooler in the unit. The hydrogen concentration is hourly monitored by the ATG-6118H automatic analyzer from 0.01 to 1000 ppm with precision of ±5%, which was calibrated and maintained by the instrument manufacturing company (Wen et al., 2018; NOA certification, 2019). All of the gas pipeline was well sealed, which wasn't affected by the air temperature, air humidity and rainfall. The data obtained by this system are sent to the laboratory located at Beijing via 5G mobile phone signal once an hour.

RESULTS

Chemical Composition of the Hot Spring Bubbling Gas

Gas collected at the Luojishan hot spring from the bubbling pools was characterized from April 25, 2010 to April 19, 2019 in detail (isotope ratios of CO_2, He and Ne and gas composition) (**Table 1**). The temperatures of Luojishan hot spring water ranged from 43°C to 44.8°C. The N_2 concentrations of hot spring gas samples were ≥80 vol%. Gas had relatively low concentrations of H_2 (≤2 ppm) and low to the detection limit

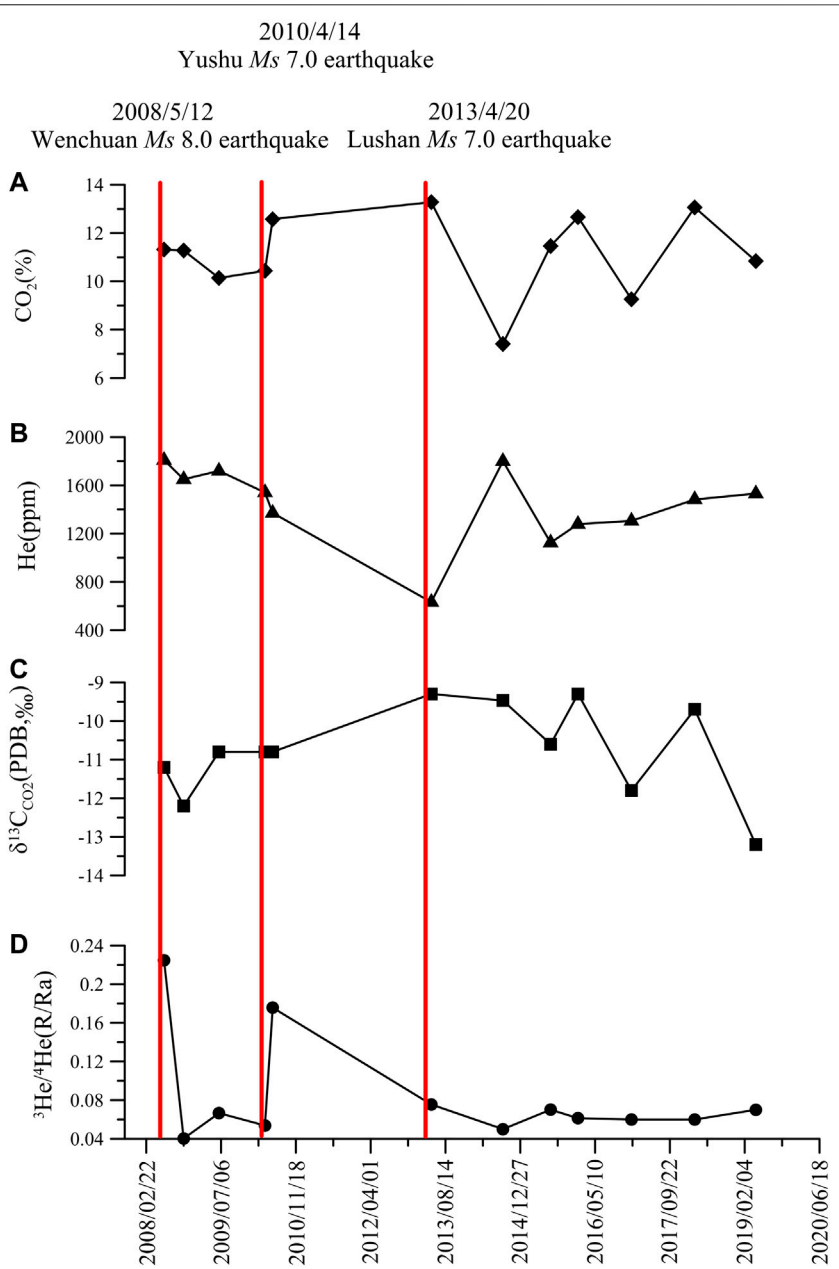

FIGURE 7 | Temporal variations of CO_2 concentration **(A)**, He concentration **(B)**, $\delta^{13}C_{CO2}$ (‰,PDB) values **(C)**, $^3He/^4He$ (R/Ra) **(D)** values in the spring gas samples.

of Macro 3000 gas chromatography. The gas samples had very higher concentrations of He (up to 1810 ppm). The concentration range of Ar in the bubbling gas was from 0.93 to 1.26%. The concentration of O_2 in the majority of bubbling gas samples was lower than 5%. Methane concentrations were lower than 1%.

He and Ne Isotopic Ratios

The $^3He/^4He$ ratios of the bubbling gas samples ranged from 0.04 to 0.22 Ra and were independent of the concentration of helium in each gas sample. **Figure 3** shows the relationships between the measured $^3He/^4He$ (R/Ra) and $^4He/^{20}Ne$ ratios. The $^4He/^{20}Ne$ and $^3He/^4He$ ratios suggest that all samples were from a mixing region with three end members: crustal-derived helium, mantle-derived helium and atmospheric helium dissolved in water. $^4He/^{20}Ne$ ratios ranged from 37.3 to 117.4, above the atmospheric background ($^4He/^{20}Ne = 0.318$, Ozima and Podosek, 1983). The $^4He/^{20}Ne$ ratios indicated that the gas samples had minimal atmospheric contamination (**Figure 3**). The Rc/Ra values are the corrected $^3He/^4He$ ratios (R/Ra) for air contamination (Jenkins, 1982; Sano and Wakita, 1985). The Rc/Ra values ranged from 0.04 to 0.17 (**Table 1**) in the bubbling gas of Luojishan hot spring.

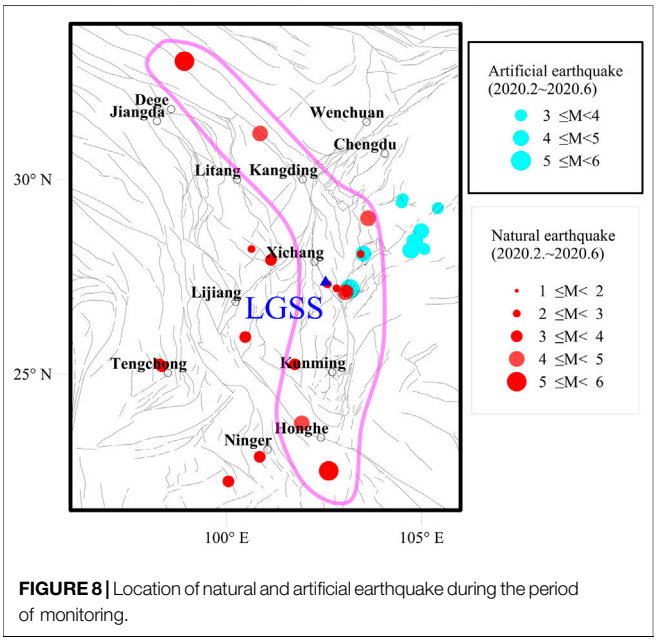

FIGURE 8 | Location of natural and artificial earthquake during the period of monitoring.

H_2 Concentration in Hot Spring Gas

There were 2813 observed values of H_2 concentration from 26 February to June 22, 2020 (**Figure 4**). The H_2 concentration ranged from 0.01 to 2.91 ppm (**Figure 4**), with average H_2 concentration, 0.13 ppm. The anomalous threshold was 0.2 ppm (**Figure 5**), which was determined by the Q-Q plot, which is a method of determining threshold values between background and anomalous geochemical data, based on partitioning a cumulative probability plot of the data (Sinclair, 1991).

DISCUSSION

Origin of He, CO_2, and H_2

He

The mixing proportion of mantle-derived He and crustal-derived He was estimated by using the Sano and Wakita (1985) equation's system (**Figure 3**). The proportion of mantle-derivd He varies from 0.47 to 2.16% at the Luojishan hot spring (**Table 1**). The radiogenic crustal-derived He was dominant in most of the bubbling gas samples in the Luojishan hot spring.

The majority of bubbling gas samples from the Luojishan hot spring have significantly lower $^3He/^4He$ signatures with $^3He/^4He$ < 0.1 Ra (mantle-derived He < 1%), (**Figure 3**, **Table 1**), indicative of crustal-derived ^4He production, with no resolvable mantle-derived contribution. The bubbling gas of Luojishan hot springs also have the highest concentrations of ^4He (**Table 1**), up to two orders of magnitude (1810 ppm) greater than the Longtougou hot springs (~5 ppm) in the Kangding city (Zhou et al., 2015).

CO_2

The end-member compositions for mantle carbon (M), sedimentary organic carbon (S) and lime stones (L) are $\delta^{13}C_{CO2}$ = −30, −6.5, and 0‰; and $^3He/^4He$ (R/Ra) = 0.02 and 8, respectively (Sano and Marty 1995). The trajectories for binary mixing between M and S, M and L, and L and S are shown in the diagram.

Combination of helium and carbon isotopes can provide more information of the carbon sources (Hilton, 1996). The main sources of carbon include the marine limestones, upper-mantle degassing, and the oxidation of organic carbon from sedimentary rocks. These main carbon sources have distinct $\delta^{13}C$ end-members, whereby upper-mantle degassing ranges between −9 and −4‰, sedimentary organic matter has $\delta^{13}C$ close to −30‰ and marine limestone has $\delta^{13}C$ close to 0‰ (Sano and Marty, 1995). **Figure 6** shows the analytical results of Luojishan hot spring gas. It is then clear that all Luojishan hot spring gas are plotted within the two mixing lines.This feature strongly suggests that CO_2 in Luojishan hot spring gases is released from three different sources: crustal metamorphic, mantle and organic components.

H_2

The origins of the hydrogen are most likely attributed to: **(A)** hydrogen generation from water-rock reactions. The abiotic H_2 is generated by the reaction of water with ultrabasic rocks or serpentinization under near-surface conditions and migration from the deep reservoirs (Lollar et al., 2014; Parnell and Blamey, 2017; Irfan et al., 2019; Wang et al., 2019; Wang et al., 2020), **(B)** the interaction of water with freshly exposed rock surfaces (Hirose et al., 2011), **(C)** mixing with the considerable amount of microbial H_2 from the biological activity and decomposition of organic matter (Prinzhofer et al., 2019; Myagkiy et al., 2020).

Temporal Variations of $^3He/^4He$ and $\delta^{13}C$ Values

The $\delta^{13}C_{CO2}$ values evidently increased from 2008 to 2016 in the Luojishan hot spring, whereas afterward, they showed an opposite trend from 2016 to 2019. These indicated that the proportion of CO_2 derived from limestone increased in the bubbling gas of Luojishan hot springs, which were related with the enhanced degassing of the triggering of the Wenchuan *Ms* 8.0 earthquake, Yushu *Ms* 7.0 earthquake and Lushan *Ms* 7.0 earthquake (**Figure 7**). The clear decrease of the $\delta^{13}C_{CO2}$ values measured from 2016 to 2019 would imply decrease of CO_2 derived from limestone and the relative increase of CO_2 from sedimentary organic, which is back to background level before Wenchuan *Ms* 8.0 earthquake. Due to the higher content of helium in the Luojishan hot spring gas, the $^3He/^4He$ ratios drop from 0.22 Ra down to 0.07 Ra from June 20, 2008 to June 22, 2009 at the Luojishan hot spring was observed after the Wenchuan *Ms* 8.0 earthquake due to the release of crustal-derived components. The $^3He/^4He$ ratios increased on June 16, 2010 after Yushu *Ms* 7.0 earthquake (April 14, 2010) in Luojishan hot spring, but He, CO_2 concentration and $\delta^{13}C_{CO2}$ isotope changed weakly. This is attributable to distance of epicenter 800 km. Yushu *Ms* 7.0 earthquake could trigger limitedly crustal-derived ^4He and CO_2, and

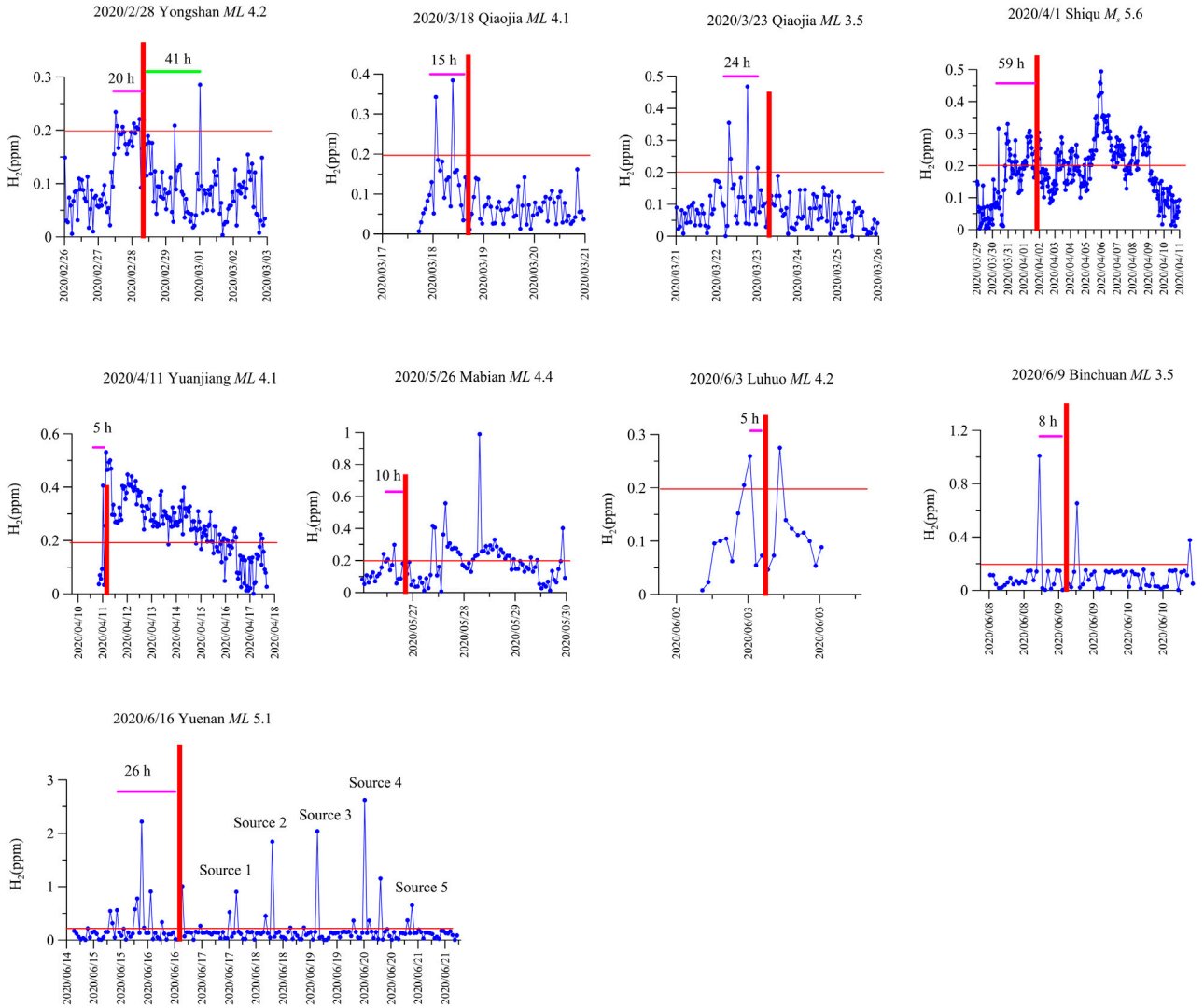

FIGURE 9 | Precursor anomalies induced by natural earthquake.

$\delta^{13}C_{CO2}$ isotope. The mantle-derived He was sensitive to Yushu *Ms* 7.0 earthquake. The $^{3}He/^{4}He$ ratios weakly increased after Lushan *Ms* 7.0 earthquake. The mantle-derived helium in the bubbling gas of hots springs was estimated that up to 62% in the Kangding region in June 2008 after Wenchuan *Ms* 8.0 earthquake. Over time, the proportion of the mantle-derived fluid contribution to the bubbling gas gradually decreased, but the crustal-derived gas components: CO_2 and CH_4 derived from organic matter and radiogenic He increased (Zhou et al., 2015). The Longtougou and Luojishan hot spring are in same strain field (XSHF, ANHF, ZMHF, XJF), which is a huge left-lateral strike-slip active fault system. A maximum shear strain rate of 40–60 nanostrain/yr is found along the XSHF-XJF system, which delineates the north and east boundaries of the crustal materials undergoing large-scale clockwise rotation around the eastern Himalaya syntaxis (Wang and Shen, 2020). The earthquake may play a very important role in He degassing in bubbling gas of hot spring from the active faults (Sano et al., 1998).

Temporal Variations of Hydrogen Concentration

Natural Earthquake Induced Precursor Anomalies

There were obvious short-term (5–60 h) seismic precursor anomalies of H_2 concentration of the Luojishan hot spring gas before some natural earthquakes from 26 February to June 21, 2020 (**Figures 8**, **9**, **Table 2**). When the stress increase up to sub-instability stress state of the faults in the XSHF-XJF system, earthquakes were occurred (Ma, 2016). The concentration of hydrogen in bubbling gas is sensitive to increase of stress in the XSHF-XJF system, which could enhance the opening of microfractures under the Luojishan

TABLE 2 | Seismic data is related to natural and artificial earthquakes recorded during the course of monitoring.

Time	Artificial earthquake	Natural earthquake	Location	Epicentral distance	Longitude	Latitude	Focal depth	Duration of preseismic precursor (h)	Types of earthquake	
(YYYY/MM/DD HH:mm)	Magnitude	Magnitude			(km)	(°)	(°)	(km)	(h)	
2020/2/28 7:56		4.2	ML	Yongshan	122.6	103.510	28.090	12	20	N
2020/3/5 13:23		3.8	ML	Muli	150.0	101.140	27.930	11		N
2020/3/17 10:30	4.1		ML	Changning	279.0	104.990	28.670	10		I
2020/3/18 16:43		4.1	ML	Qiaojia	60.3	103.050	27.100	8	15	N
2020/3/23 7:10		3.5	ML	Qiaojia	61.7	103.080	27.120	8	24	N
2020/3/27 13:07		3.6	ML	Simao	531.4	100.850	22.870	13	15	N
2020/4/1 20:23		5.6	Ms	Shiqu	717.2	98.920	33.040	10	59	N
2020/4/6 15:01	3.3		ML	Xingwen	264.7	105.070	28.210	8		I
2020/4/8 6:06		2.3	ML	Puge	6.3	102.540	27.341	8		N
2020/4/9 9:14	3.8		ML	Junlian	229.8	104.720	28.140	8		I
2020/4/11 4:03		4.1	ML	Yuanjiang	412.4	101.930	23.730	9	5	N
2020/4/11 23:19		2.3	ML	Puge	11.1	102.594	27.310	16		N
2020/4/12 11:06	3.5		ML	Rongxian	294.0	104.490	29.410	8	15	I
2020/4/14 5:10		3.7	ML	Lancang	626.1	100.050	22.240	11		N
2020/4/14 12:00		2.3	ML	Puge	11.7	102.598	27.306	14		N
2020/4/14 12:01		2.1	ML	Puge	10.0	102.565	27.311	15		N
2020/4/15 1:39		3.7	ML	Tengchong	484.7	98.340	25.200	13		N
2020/4/15 1:46		3.6	ML	Tengchong	487.1	98.280	25.250	12		N
2020/4/15 11:35	3.6		ML	Luxian	349.8	105.420	29.260	8		I
2020/4/23 17:04	4.1		ML	Changning	253.0	104.840	28.420	8		I
2020/4/27 9:37	3.8		ML	Gongxian	236.9	104.780	28.180	9		I
2020/4/27 20:19	3.9		ML	Qiaojia	65.0	103.150	27.180	11		I
2020/5/10 15:42	4		ML	Gongxian	232.8	104.740	28.170	11		I
2020/5/11 6:09	3.6		ML	Changning	247.9	104.770	28.440	10		I
2020/5/14 9:41		2.9	ML	Leibo	116.6	103.440	28.080	117		N
2020/5/18 21:47	5		Ms	Qiaojia	65.9	103.160	27.180	8		R
2020/5/19 4:35	3.8		ML	Qiaojia	65.9	103.160	27.180	8		R
2020/5/22 3:12	4.2		ML	Gongxian	230.5	104.710	28.180	8		I
2020/5/22 20:32		3.3	ML	Lufeng	251.5	101.750	25.250	15		N
2020/5/25 0:01	3.4		ML	Gongxian	234.4	104.770	28.140	8		I
2020/5/26 20:34		4.4	ML	Muchuan	207.7	103.630	29.000	14	10	N
2020/5/30 8:30	3.5		ML	Yongshan	122.7	103.520	28.080	11		N
2020/5/31 12:25	3.7		ML	Gongxian	234.5	104.740	28.210	8		I
2020/6/1 12:42	3.8		ML	Junlian	229.8	104.720	28.140	8		I
2020/6/2 16:39	3.9		ML	Gongxian	231.8	104.720	28.190	13		I
2020/6/3 2:57		4.2	ML	Luhuo	451.0	100.860	31.180	14	5	N
2020/6/5 15:49	3.2		ML	Gongxian	234.7	104.760	28.170	7		I
2020/6/9 2:39		3.5	ML	Binchuan	260.4	100.480	25.950	9	8	N
2020/6/10 3:03		2.1	ML	Ningnan	35.3	102.820	27.200	17		N
2020/6/10 10:20	3.4		ML	Gongxian	238.0	104.760	28.250	9		I
2020/6/10 21:08		1.5	ML	Puge	2.2	102.530	27.380	4		N
2020/6/11 4:29		2.9	ML	Muli	207.5	100.640	28.210	16		N
2020/6/11 7:47	3.6		ML	Rongxian	302.6	104.520	29.490	9		I
2020/6/11 10:25	3.4		ML	Gongxian	232.4	104.740	28.160	7		I
2020/6/12 21:03	4		ML	Gongxian	232.7	104.730	28.190	8		I
2020/6/13 10:32	3.5		ML	Gongxian	237.7	104.780	28.200	9		I
2020/6/16 14:12		5.1	ML	Vietnam	543.6	102.620	22.510	8	26	N

N, natural earthquake; I, injection-induced seismicity; R, reservoir-induced earthquake.

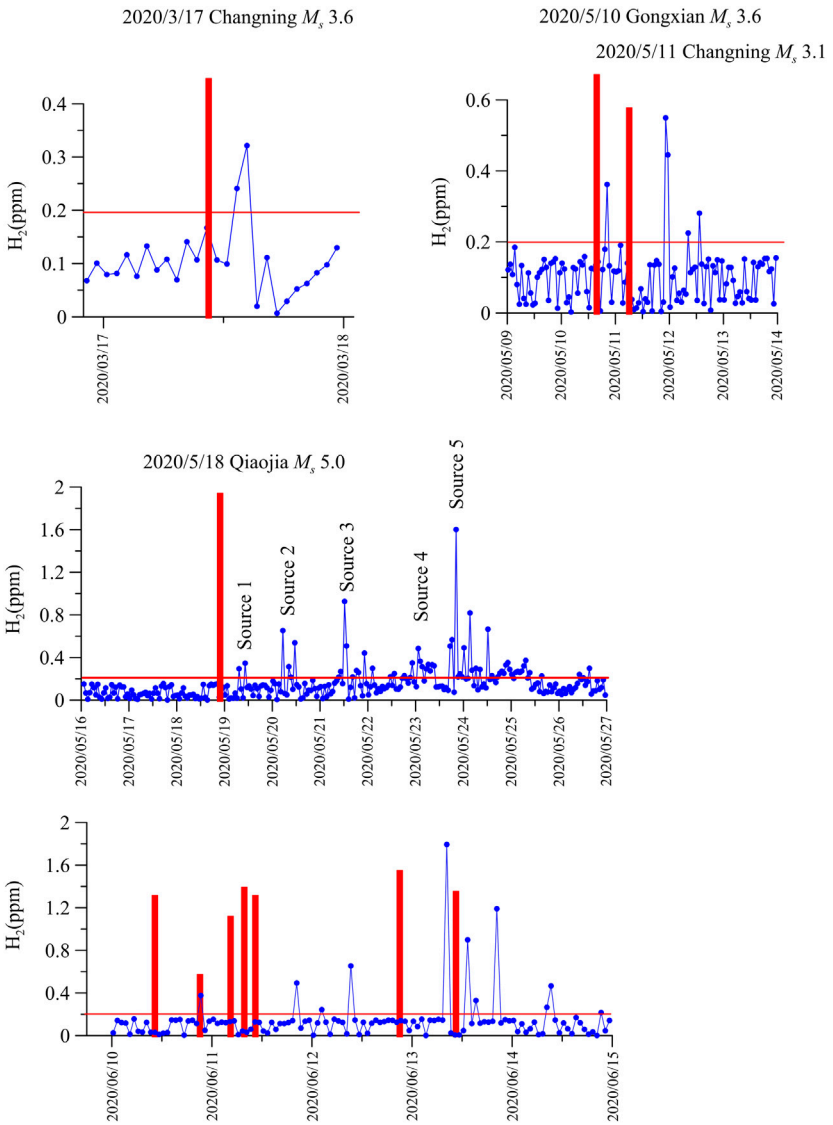

FIGURE 10 | Precursor anomalies induced by artificial earthquakes.

hot spring. According to the variation characteristics of the stress and strain, the anomalies of H_2 concentration have different characteristics. It exhibits a persistent stress increase most probably caused by a persistent contribution of the different depths and gas caused by the strain release before the natural seismic events (Cicerone et al., 2009; Crampin et al., 2015). Anomalous precursory (anomalous threshold was 0.2 ppm) changes in the diffuse emission of H_2 in hot spring have been observed before some of the micro-seismicity of the April 11, 2020 Puger earthquakes with distance of epicenter, 6.3 km. A significant increase (up to 0.32 ppm) in H_2 concentration was detected 60 h before a Shiqu *Ms* 5.6 earthquake on April 1, 2020, 717 km away from the Liojishan station. The anomalies of H_2 concentration are just one or two points of data before earthquake, which could be induced by pulsed stress increases in the XSHF-XJF system. In addition, pre- and post-seismic variations of H_2 concentration have also been observed related to the occurrence of a seismic swarm beneath ZMHF (**Figures 8**, **9**, **Table 2**).

It is suggested that observed preseismic precursor of H_2 concentration are geochemical signals of the earthquake preparation process due to stress-corrosion (Ito et al., 1999). Dynamic disturbances of frictional contacts in the fault planes by seismic waves may also account for co-and post-seismic increases in H_2 (Kita et al., 1982). Seismicity may induce permeability enhancement of fault fractures (Hirose et al., 2011). The Luojishan gas monitoring system is sensitive enough to quantify emission during periods of intense seismic activities. According to characteristic of short term precursors of H_2 concentration in Luojishan hot spring from February 23, 2020 to March 31, 2020, a day before the Shiqu *Ms* 5.6 earthquake on

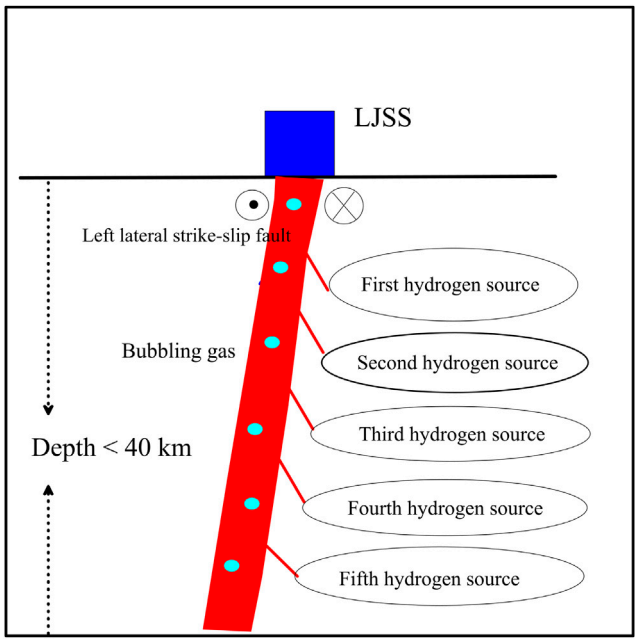

FIGURE 11 | Schematic diagram of hydrogen sources in Luojishan hot spring bubbling gas.

April 1, 2020 and Vietnam *ML*5.1 earthquake on June 16, 2020, forecasting informations (in the coming 24 h, in the eastern Tibetan Plateau, around *Ms* 5.0) were suggested to department of forcasting, institute of earthquake forcasting, China Earthquake administration. There were obvious persistent precursor anomalies of H_2 concentration of the Luojishan hot spring gas before the Shiqu *Ms* 5.6 earthquake and Vietnam M_L5.1 earthquake. The mechanism of precursor anomalies may be persistent stress increase before the natural seismic events in the XSHF-XJF system.

Hydrologic responses to earthquakes depend on earthquake magnitudes and distances from epicenters (Wang and Manga, 2010; Cox et al., 2015). Therefore it is difficult to identify short-term seismic precursory anomaly systematically by some criterias on the basis of several earthquakes (M > 5.0). After hundreds of natural earthquake (M > 5.0) were collected and analyzed, the formula about precursor anomalies and earthquake magnitude, epicentral distance may be summarized and some criterias may be provided.

Artificial Earthquake Trigger Anomalies

The earthquakes may trigger anomalies over great (>300 km) distances from the epicenter, but a robust relationship between post-seismic anomalies and seismic activity remains elusive. The relationship between a hot spring response and dynamic stresses propagated by surface waves, were demonstrated by changes in H_2 emissions measured by the gas monitoring station. The positive hot spring gas responses with the spike-like anomalies are identified if the post-earthquake H_2 mass was larger than the anomalies threshold of H_2 concentration. Micro-seismicity induced by injection in shale gas exploration in Changning (Liu et al., 2020) occurred repeatedly during the monitoring period. Qiaojia *Ms* 5.0 earthquake on May 18, 2020 was induced by Xiluodu reservoir filling (Liao et al., 2020). Artificial earthquakes (ML ≥ 3.0) triggered geochemical post-seismic anomalies were repeatedly observed (**Figure 10**, **Table 2**). The minimum artificial earthquakes, which may triggered geochemical post-seismic anomalies, can be estimated by a lot of seismic data in future.

Modeling of Migration of H_2 in Hot Spring Gas in the Zemuhe Fault

The positive post-earthquake H_2 anomalies responses with the five spike-like anomalies were observed from 18 to 25 May after Qiaojia *Ms* 5.0 earthquake on May 18, 2020 (**Figure 9**). This phenomenon were repeatedly observed after Vietnam *ML* 5.1 earthquake on June 16, 2020 (**Figure 10**). A model is developed to explain the observations of the changed mixing ratio among five hydrogen sources systems (**Figure 11**) as a result of a pressure disturbance triggered by seismic waves passing the Luojishan monitoring station. This model requires the existence of i) a mixed gas system with a high H_2 concentration contrast among the five sources with different depth in fault, ii) Five confined, stress sensitive fractures where five fluid components circulate along macro-fractures and where the gas components enter the ZMHF by diffusion through micro-fractures, iii) Five free bubbling gas phase in the fractures, and iv) a chance for free gas bubbles to rise toward the earth's surface before being trapped under an impermeable cover, which collects gas. The passing seismic waves may enhance the local pore pressure. Increased pressure changes in the mixing ratio in favor of the gas components which circulates through the macro-fractures (Kissin, 2007). Five hydrogen sources systems were simultaneously triggered by seismic waves. Hydrogen of five sources entered simultaneously into the main fracture of ZMHF. Since the depth of five hydrogen sources were different, the time of arrival of Hydrogen of five sources were diferent. The model provides a plausible physical and chemical explanations for the anomalies triggered by earthquake. There are a lot of free parameters in the model which are poorly resolved. Because helium isotope ratios (R/Ra) of the gas samples was 0.07 Ra on April 19, 2019, the ZMHF was a conduit for dominant crustal-derived fluid. The depth of Moho surface is ~40 km (Teng et al., 2014). The H_2 coming from fifth source migrated upward monitoring station during five days. The ascending velocity of H_2 is difficultly estimated. The depth of the fifth source of H_2 is shallower than 40 km.

CONCLUSION

1) Helium isotope ratios in Luojishan hot springs gas varied from 0.05 to 0.18 Ra, with mantle-derived He up to 2.2% in the Luojishan hot spring indicated the radiogenic crustal-derived He was dominant in most of the bubbling gas samples in the Luojishan hot spring. N_2 concentrations were ≥80 vol% and O_2 contents were lower than 5% in the majority of hot spring gas samples.

2) The time series of hydrogen concentration display a complex temporal pattern reflecting a wide range of different physical processes. There were clear short-term (5–60 h) seismic precursor anomalies of hydrogen concentration related with the epicentral distance and magnitude of earthquake before natural earthquake, with post-seismic response. The artificial earthquake only induced the post-seismic responses.
3) Monitoring the hydrogen concentrations with automatic gas stations may be promising tool for unraveling earthquake mechanisms and for predicting earthquakes. More parameters (He, CO_2, water temperature) may be monitored in the future studies to get a better insight into the possible relationships between earthquakes and gas geochemistry.

DATA AVAILABILITY STATEMENT

The raw data supporting the conclusions of this article will be made available by the authors, without undue reservation.

AUTHOR CONTRIBUTIONS

All authors have made a substantial, direct, and intellectual contribution to the work and approved it for publication.

FUNDING

This research was supported by National Key Research and Development Project (2017YFC1500501) and, the National Natural Science Foundation of China (41673106), The Special Fund of the Institute of Earthquake Forecasting, China Earthquake Administration (2017IES010205, 2016IES010304, 2018IEF010104, 2020IEF0604, 2020IEF0703).

ACKNOWLEDGMENTS

The authors are grateful to Prof. Fang Du and Prof. Hong Fu for her assistance with field work.

REFERENCES

Babuška, V., Růžek, B., and Dolejš, D. (2016). Origin of earthquakes warms in the western Bohemian Massif:Is the mantle CO_2 degassing, followed by the Cheb Basin subsidence, an essential driving force?. *Tectonophysics* 668–669, 42–51. doi:10.1016/j.tecto.2015.12.008

Ballentine, C. J., Marty, B., Sherwood Lollar, B., and Cassidy, M. (2005). Neon isotopes constrain convection and volatile origin in the Earth's mantle. *Nature* 433, 33–38. doi:10.1038/nature03182

Cao, C. H., Zhang, M. J., Tang, Q. Y., Yang, Y., Lv, Z. G., Zhang, T. W., et al. (2018). Noble gas isotopic variations and geological implication of Longmaxi shale gas in Sichuan Basin, China. *Mar. Petrol. Geol.* 89, 38–46. doi:10.1016/j.marpetgeo.2017.01.022

Cicerone, R. D., Ebel, J. E., and Britton, J. (2009). A systematic compilation of earthquake precursors. *Tectonophysics* 476 (3–4), 371–396. doi:10.1016/j.tecto.2009.06.008

Cox, S. C., Menzies, C. D., Sutherland, R., Denys, P. H., Chamberlain, C., and Teagle, D. A. H. (2015). Changes in hot spring temperature and hydrogeology of the Alpine Fault hanging wall, New Zealand, induced by distal South Island earthquakes. *Geofluids* 15, 216–239. doi:10.1111/gfl.12093

Crampin, S., Gao, Y., and Bukits, J. (2015). A review of retrospective stress-forecasts of earthquakes and eruptions. *Phys. Earth Planet. In.* 24, 76–87. doi:10.1016/j.pepi.2015.05.008

Donald, T. (1988). Geochemical precursors to seismic activity. *Pure Appl. Geophys* 126 (2-4), 241–266.

Fischer, T., Matyska, C., and Heinicke, J. (2017). Earthquake-enhanced permeability-evidence from carbon dioxide release following the M_L 3.5 earthquake in West Bohemia. *Earth Planet Sci. Lett.* 460, 60–67. doi:10.1016/j.epsl.2016.12.001

Gherardi, F., Pierotti, L., and Vista, A. D. (2017). Water-rock interactions in a site investigated for geochemical precursors of earthquakes: the pieve fosciana spring (Italy). *Earth Planet Sci. Lett.* 17, 360–363. doi:10.1016/j.proeps.2016.12.091

Graham, D. W. (2002). "Noble gas isotope geochemistry of mid-ocean ridge and ocean island basalts: characterization of mantle source reservoirs," in *Noble gases in geochemistry and cosmochemistry, reviews in mineralogy and geochemistry* (Washington), Vol. 47(1), 247–317. doi:10.2138/rmg.2002.47.8

Gupta, H. K. (2001). Short-term earthquake forecasting may be feasible at Koyna, India. *Tectonophysics* 338 (3–4), 353–357. doi:10.1016/s0040-1951(01)00083-x

He, H., and Oguchi, T. (2008). Late Quaternary activity of the Zemuhe and Xiaojiang faults in southwest China from geomorphological mapping. *Geomorphology* 96, 62–85. doi:10.1016/j.geomorph.2007.07.009

Hilton, D. R. (1996). The helium and carbon isotope systematics of a continental geothermal system: results from monitoring studies at Long Valley Caldera (California, U.S.A). *Chem. Geol.* 127, 269–295. doi:10.1016/0009-2541(95)00134-4

Hilton, D. R. (2007). Geochemistry. The leaking mantle. *Science* 318, 1389–1390. doi:10.1126/science.1151983

Hirose, T., Kawagucci, S., and Suzuki, K. (2011). Mechanoradical H_2 generation during simulated faulting: Implications for an earthquake-driven subsurface biosphere. *Geophys. Res. Lett.* 38, L17303. doi:10.1029/2011gl048850

Huang, F., Li, M., Ma, Y., Han, Y., Tian, L., Yan, W., et al. (2017). Studies on earthquake precursors in China: A review for recent 50 years. *Geod Geodyn.* 8 (1), 1–12. doi:10.1016/j.geog.2016.12.002

Irfan, M., Zhou, L., Bai, Y., Yuan, S., Liang, T. T., Liu, Y. F., et al. (2019). Insights into the hydrogen generation from water-iron rock reactions at low temperature and the key limiting factors in the process. *Int. J. Hydrogen Energy* 44 (33), 18007–18018. doi:10.1016/j.ijhydene.2019.05.086

Ito, T., Nagamine, K., Yamamoto, K., Adachi, M., and Kawabe, I. (1999). Preseismic hydrogen gas anomalies caused by stress-corrosion process preceding earthquakes. *Geophys. Res. Lett.* 26 (13), 2009–2012. doi:10.1029/1999gl900407

Jenkins, W. J. (1982). Tritium and ^{3}He in the Sargasso Sea. *J. Mar. Res.* 40, 533–569

King, C. Y. (1986). Gas geochemistry applied to earthquake prediction: an overview. *J. Geophys. Res.* 91, 12269–12281. doi:10.1029/jb091ib12p12269

Kissin, I. G. (2007). New data on crustal sensitive zones and formation of precursors and postseismic responses to earthquakes. *Russ. Geol. Geophys.* 48 (5), 429–441. doi:10.1016/j.rgg.2005.12.001

Kita, I., Matuo, S., and Wakita, H. (1982). H_2 generation by reactionbetween H_2O and crushed rock:An experimental study on H_2 degassing from the active fault zone. *J. Geophys. Res.* 87 (B13), 10789–10795. doi:10.1029/jb087ib13p10789

Li, Z. P., Wang, X. B., Li, L. W., Zhang, M. J., Tao, M. X., Xing, L. T., et al. (2014). Development of new method of δ^{13}C measurement for trace hydrocarbons in natural gas using solid phase micro-extraction coupled to gas chromatography isotope ratio mass spectrometry. *J. Chromatogr. A* 1372, 228–235. doi:10.1016/j.chroma.2014.10.089

Liao, L., Li, P., Yang, J., and Feng, J. (2020). The simulation of rupture dynamics from potential earthquakes around XiLuoDu reservoir dam, China. *Phys. Earth Planet. In.* 302, 106488. doi:10.1016/j.pepi.2020.106488

Liu, J., and Zahradník, J. (2020). The 2019 MW 5.7 changning earthquake, China: a shallow doublet with different faulting styles. Geophys. *Res. Lett*. 47. doi:10.1029/2019GL085408

Lollar, B. S., Onstott, T. C., Lacrampe-Couloume, G., and Ballentine, C. J. (2014). The contribution of the Precambrian continental lithosphere to global H2 production. *Nature* 516, 379–382. doi:10.1038/nature14017

Ma, J. (2016). On "whether earthquake precursors help for prediction do exist". *Chin. Sci. Bull.* 61, 409–414 [in Chinese]. doi:10.1360/n972015-01239

Myagkiy, A., Brunet, F., Popov, C., Krüger, R., Guimarães, H., Sousa, R. S., et al. (2020). H_2 dynamics in the soil of a H_2-emitting zone (São Francisco Basin, Brazil): Microbial uptake quantification and reactive transport modelling. *Appl. Geochem.* 112, 104474. doi:10.1016/j.apgeochem.2019.104474

Nagamine, K. (1994). Origin and coseismic behavior of mineral spring gas at Byakko, Japan, studied by automated gas chromatographic analyses. *Chem. Geol.* 114 (1–2), 3–17. doi:10.1016/0009-2541(94)90038-8

NOA certification (2019). Validity of the certificate:2019/7/25~2020/7/25. Certificate Number:NOA1994077. Available at: http://www.noagroup.org/certificate, http://cx.cnca.cn/CertECloud/result/skipResultList

Ozima, M., and Podosek, F. A. (1983). *Noble gas geochemistry*. Cambridge: Cambridge University Press, 367.

Parnell, J., and Blamey, N. (2017). Global hydrogen reservoirs in basement and basins. *Geochem. Trans.* 18, 2. doi:10.1186/s12932-017-0041-4

Prinzhofer, A., Moretti, I., Françolin, J., Pacheco, C., D'Agostino, A., Werly, J., et al. (2019). Natural hydrogen continuous emission from sedimentary basins: The example of a Brazilian H_2-emitting structure. *Int. J. Hydrogen Energy* 44 (12), 5676–5685. doi:10.1016/j.ijhydene.2019.01.119

Ren, Z., Lin, A., and Rao, G. (2010). Late Pleistocene–Holocene activity of the Zemuhe Fault on the southeastern margin of the Tibetan Plateau. *Tectonophysics* 495 (3–4), 324–336. doi:10.1016/j.tecto.2010.09.039

Sano, Y., and Marty, B. (1995). Origin of carbon in fumarolic gas from island arcs. *Chem. Geol.* 119 (1-4), 265–274. doi:10.1016/0009-2541(94)00097-r

Sano, Y., Takahata, N., Igarashi, G., Koizumi, N., and Sturchio, N. (1998). Helium degassing related to the Kobe earthquake. *Chem. Geol.* 150 (1-2), 171–179. doi:10.1016/s0009-2541(98)00055-2

Sano, Y., and Wakita, H. (1985). Geographical distribution of $^3He/^4He$ ratios in Japan: implications for arc tectonics and incipient magmatism. *J. Geophys. Res.* 90 (B10), 8729–8741. doi:10.1029/jb090ib10p08729

Sato, M., Sutton, A. J., McGee, K. A., and Russell-Robinson, S. (1986). Monitoring of hydrogen along the San Andreas and Calaveras faults in central Californiain 1980-1984. *J. Geophys. Res.* 91 (B12), 12315–12326. doi:10.1029/jb091ib12p12315

Sinclair, A. J. (1991). A fundamental approach to threshold estimation in exploration geochemistry: Probability plots revisited. *J. Geochem. Explor.* 41 (1-2), 1–22. doi:10.1016/0375-6742(91)90071-2

Sugisaki, R., Ido, M., Takeda, H., Isobe, Y., Hayashi, Y., Nakamura, N., et al. (1983). Origin of hydrogen and carbon dioxide in fault gases and its relation to fault activity. *J. Geol.* 91 (3), 239–258. doi:10.1086/628769

Sugisaki, R., Ito, T., Nagamine, K., and Kawabe, I. (1996). Gas geochemical changes at mineral springs associated with the 1995 southern Hyogo earthquake (M = 7.2), Japan. *Earth Planet Sci. Lett.* 139 (1-2), 239–249. doi:10.1016/0012-821x(96)00007-6

Sugisaki, R., and Sugiura, T. (1986). Gas anomalies at three mineral springs and a fumarole before an inland earthquake, central Japan. *J. Geophys. Res.* 91 (B12), 12296–12304. doi:10.1029/jb091ib12p12296

Teng, J., Deng, Y., Badal, J., and Zhang, Y. (2014). Moho depth, seismicity and seismogenic strcture in China mainland. *Tectonphysics* 627, 108–121. doi:10.1016/j.tecto.2013.11.008

Umeda, K., Asamori, K., and Kusano, T. (2013). Release of mantle and crustal helium from a fault following an inland earthquake. *Appl. Geochem.* 37, 134–141. doi:10.1016/j.apgeochem.2013.07.018

Wakita, H., Nakamura, Y., Kita, I., Fujii, N., and Notsu, K. (1980). Hydrogen release: New indicator of fault activity. *Science* 210, 188–190. doi:10.1126/science.210.4466.188

Wang, C. Y., and Manga, M. (2010). Hydrologic responses to earthquakes and a general metric. *Geofluids* 10, 206–216. doi:10.1111/j.1468-8123.2009.00270.x

Wang, J., Watanabe, N., Okamoto, A., Nakamura, K., and Komai, T. (2019). Acceleration of hydrogen production during water-olivine-CO_2 reactions via high-temperature-facilitated Fe(II) release. *Int. J. Hydrogen Energy* 44 (23), 11514–11524. doi:10.1016/j.ijhydene.2019.03.119

Wang, J., Watanabe, N., Okamoto, A., Nakamura, K., and Komai, T. (2020). Characteristics of hydrogen production with carbon storage by CO_2-rich hydrothermal alteration of olivine in the presence of Mg–Al spinel. *Int. J. Hydrogen Energy* 45 (24), 13163–13175. doi:10.1016/j.ijhydene.2020.03.032

Wang, M., and Shen, Z. K. (2020). Present-day crustal deformation of continental China derived from GPS and its tectonic implications. *J. Geophys. Res.: Solid Earth* 125, e2019JB018774. doi:10.1029/2019JB018774

Weinlich, F. H., Gaždová, R., Teschner, M., and Poggenburg, J. (2016). The October 2008 Nový Kostel earthquake swarm and its gas geochemical precursor. *Geofluids* 16 (5), 826–840. doi:10.1111/gfl.12187

Wen, L., He, L., Feng, E., Lian, K., Chen, Q., Zhang, L., et al. (2018). Calibration, Performance Testing and Their Results of the Automatic Trace Hydrogen Analyzer ATG-6118H. *Earthq. Res. China* 34 (3), 571–579 [in Chinese with English abstract].

Wen, X., Ma, S., Xu, X., and He, Y. (2008). Historical pattern and behavior of earthquake ruptures along the eastern boundary of the Sichuan-Yunnan faulted-block, southwestern China. *Phys. Earth Planet. In.* 168 (1-2), 16–36. doi:10.1016/j.pepi.2008.04.013

Zgonnik, V. (2020). The occurrence and geoscience of natural hydrogen: A comprehensive review. *Earth Sci. Rev.* 203, 103–140. doi:10.1016/j.earscirev.2020.103140

Zhang, P. (2013). A review on active tectonics and deep crustal processes of the Western Sichuan region, eastern margin of the Tibetan Plateau. *Tectonophysics* 584, 7–22. doi:10.1016/j.tecto.2012.02.021

Zhou, X., Wang, W., Chen, Z., Yi, L., Liu, L., Xie, C., et al. (2015). Hot spring gas geochemistry in western Sichuan Province, China after the Wenchuan *Ms* 8.0 earthquake. *Terr. Atmos. Oceanic Sci.* 26 (4), 361–373. doi:10.3319/tao.2015.01.05.01(tt)

Zhou, X., Liu, L., Chen, Z., Cui, Y., and Du, J. (2017). Gas geochemistry of the hot spring in the Litang fault zone, Southeast Tibetan Plateau. *Appl. Geochem.* 79, 17–26. doi:10.1016/j.apgeochem.2017.01.022

Zhou, X., Wang, W., Li, L., Hou, J., Xing, L., Li, Z., et al. (2020). Geochemical features of hot spring gases in the Jinshajiang-Red River fault zone, Southeast Tibetan Plateau. *Acta Petrol. Sin*. 36 (7), 2197–2214 [in Chinese with English abstract]. doi:10.18654/1000-0569/2020.07.18

Conflict of Interest: The authors declare that the research was conducted in the absence of any commercial or financial relationships that could be construed as a potential conflict of interest.